



Article

Revealing the Effects of Three Different Antimicrobial Agents on *E. coli* Biofilms by Using Soft-Probe Scanning Electrochemical Microscopy

Sorour Darvishi ^{1,2,*} and Hubert H. Girault ³

¹ Department of Electrical Engineering and Computer Sciences, University of California, Berkeley, CA 94720, USA

² Berkeley Sensor and Actuator Center, University of California, Berkeley, CA 94720, USA

³ Institute of Chemical Sciences and Engineering, Ecole Polytechnique Fédérale de Lausanne (EPFL), Station 6, 1015 Lausanne, Switzerland

* Correspondence: sorourdarvishi@gmail.com

Abstract: This paper evaluated the use of soft-probe scanning electrochemical microscopy complementarily with confocal laser scanning microscopy to study the effects of different antimicrobial agents and treatments on *E. coli* DH5 α biofilm. The antimicrobial agents were sodium azide, silver nanoparticles, and a flashlight. The effects of these agents were monitored by measuring the change in biofilm properties, such as biofilm biomass, live/dead studies, and surface activity. The results showed that sodium azide, silver nanoparticles, and the flashlight effectively killed *E. coli* biofilms and explained the mode of action for each treatment. Sodium azide was more effective in killing the biofilm after a short treatment time by blocking the ATPase, while silver nanoparticles were more effective at killing the biofilm after longer treatment times through several antibiofilm actions. This work showed that scanning electrochemical microscopy (SECM) is a very valuable tool for studying the effects of antimicrobial agents on biofilms. SECM is a sensitive technique that can be used to monitor the changes in biofilm properties in real-time. Additionally, SECM does not require any sample preparation, which makes it a convenient and efficient technique. Overall, the results of this study could be used to develop new strategies for treating *E. coli* biofilm infections and provide valuable insights into the use of SECM to study the effects of antimicrobial agents on *E. coli* biofilms.

Keywords: scanning electrochemical microscopy; confocal laser scanning microscopy; antibiofilm treatment; sodium azide; silver nanoparticle; flashlight



Citation: Darvishi, S.; Girault, H.H. Revealing the Effects of Three Different Antimicrobial Agents on *E. coli* Biofilms by Using Soft-Probe Scanning Electrochemical Microscopy. *Appl. Nano* **2023**, *4*, 260–279. <https://doi.org/10.3390/aplnano4030015>

Academic Editor: Giacomo Dacarro

Received: 17 July 2023

Revised: 18 August 2023

Accepted: 30 August 2023

Published: 4 September 2023



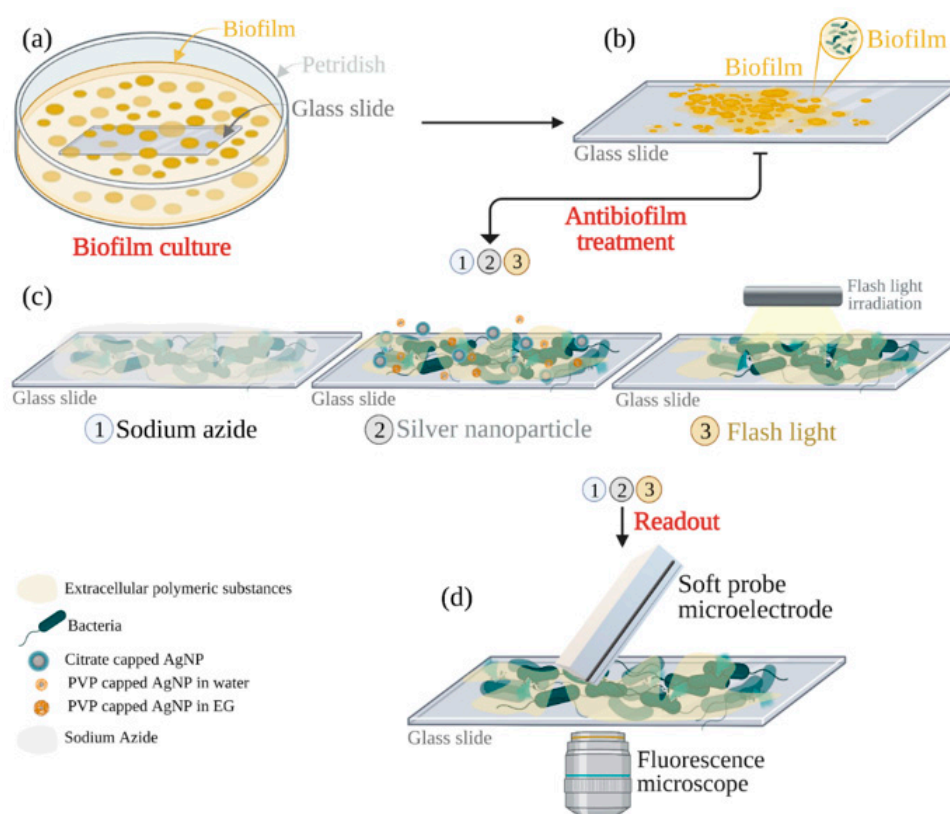
Copyright: © 2023 by the authors. Licensee MDPI, Basel, Switzerland. This article is an open access article distributed under the terms and conditions of the Creative Commons Attribution (CC BY) license (<https://creativecommons.org/licenses/by/4.0/>).

1. Introduction

Bacterial biofilms are thin organic layers of one or more bacterial cells embedded in a matrix containing extracellular polymeric substances (EPS) and water [1]. The EPS-based matrix behaves as a physicochemical barrier, limiting the accessibility of nutrient supplements and antimicrobial reagents [2]. The lack of nutrients reduces the metabolism of bacteria deep inside the biofilm, and they adapt to a dormant state, making them less susceptible to antimicrobial agents [3]. The efficiency of antibiofilm treatments is determined by detecting the bacterial cell viability embedded in the biofilm when exposed to antimicrobial agents. Several techniques can be applied to assess biofilm viability based on the biofilm's culturability, RNA detection, metabolic activity, or the determination of membrane integrity [4]. Metabolic assays detect metabolic compounds produced or consumed by bacteria, either using in situ or ex situ methods. This approach evaluates the viability of intact biofilms and can be realized by utilizing metabolic indicator dyes such as resazurin [5,6], fluorescein diacetate [7], or pH indicators [8]. Metabolic assays often evaluate the free-floating bacteria and the bacteria within the biofilm differently. This could be the main drawback of the metabolic assays for detecting biofilm viability [9].

Alternatively, electrochemical methods can be applied for the in situ investigation of the metabolic activity of biofilms. Electrochemical detection is sensitive, can be non-destructive to living biological samples, is operational in small sample volumes, can be applied in portable devices (e.g., sensors), and is generally less prone to interferences than optical methods [10–14]. As recently reviewed, electrochemical investigations of biofilms with microelectrodes offer many opportunities [15]. In particular, scanning electrochemical microscopy (SECM) is attractive for the real-time detection of redox-active small molecules and a biofilm's metabolic activity with micrometer resolution. SECM is a technique that uses a scanning probe to measure the electrochemical activity of a surface. This can be used to map the distribution of electroactive species on a surface or to study the kinetics of electrochemical reactions. SECM is a very sensitive technique that can image surfaces at the nanoscale. SECM has been used for different investigations on biofilms, e.g., the detection of H₂O₂ on biofilms, used to study the glucose metabolism of various biofilms [16,17], catalase activity of *Vibrio fischeri* biofilms [16], and quorum sensing molecules with the aid of the detection of pyocyanin [18–20]. Also, SECM was proposed to detect the effect of antimicrobial treatments [21–24]. Several chemical and physical methods have demonstrated antimicrobial effects on biofilms, including antibiotics, various materials, heat treatment, light treatment, or filtration [25–27]. Metal nanoparticles such as gold (AuNPs) and silver (AgNPs) possess an intrinsic antimicrobial activity [28]. This study used silver nanoparticles as antimicrobial agents. Furthermore, antimicrobial chemicals, including fluoride [29], chlorine [30], chlorhexidine [31], and sodium azide [32], were used to eradicate biofilms. Among the antimicrobial chemicals, azide has a significant effect as an inhibitory agent on bacteria's metabolic pathways within the biofilm [32,33]. Furthermore, the effect of light on biofilms is a complex topic, but research suggests that light can be a powerful tool for controlling the growth and spread of bacteria. The type of light, the intensity of the light, and the duration of exposure all affect the growth and behavior of biofilms [34,35]. Blue and red light (wavelengths of 400–500 and 600–700 nm, respectively) are the most effective at killing bacteria in biofilms because they can penetrate the biofilm and reach the bacteria inside. Blue light is more effective at killing bacteria than red light, but it is also more likely to damage human cells [36,37]. Green and yellow light (wavelengths of 500–600 nm) are less effective at killing bacteria in biofilms, but they can still have some effect. These wavelengths of light do not penetrate the biofilm as well as blue and red light, but they can still damage the bacteria on the surface of the biofilm. UV light (wavelengths of 200–300 nm) is also effective at killing bacteria in biofilms, but it can also damage human cells [38,39]. UV light damages the DNA of bacteria, which can prevent them from reproducing. The intensity of the light also affects its effect on biofilms [40,41]. In general, higher intensity light is more effective at killing bacteria, but too much light can damage human cells [42].

Previously, the potential to use Soft-Probe-SECM for the investigation of the metabolic activity of biofilms by utilizing the feedback mode of SECM has been demonstrated [43]. Here, the objectives were to determine the inherent impacts of antimicrobial reagents on the biofilm of the model bacterium *E. coli* strain DH5 α by recording the electrochemical surface reactivity of biofilm and to find whether the Soft-Probe-SECM is sensitive to the impact of the incubation time and concentration of antimicrobial reagents on the biofilms. We present the use of SECM to visualize the response of *E. coli* biofilms to three different antimicrobial treatments—antimicrobial reagents, including sodium azide, silver nanoparticles, flashlight treatment—and the constraints of combining and comparing with data obtained from state-of-the-art biofilm detection methods. Further, since nanoparticle transport in the biofilm is affected by particle size and aggregation state, the treatment effects of using three types of AgNPs with different colloidal stability were compared (Scheme 1). The existing literature on antimicrobial biofilm treatments has focused on single microscopy readouts. However, this study is the first to investigate the complementary detection of scanning electrochemical microscopy and confocal laser scanning microscopy. This is significant because biofilms have very complex structures, and it is crucial to have different readouts for each individual system.



Scheme 1. Workflow. (a) Biofilm culture. (b) Removing the glass slide from the cultured environment in the petri dish. Biofilm is formed on the glass slide. (c) Antibiofilm treatments including (1) sodium azide, (2) silver nanoparticle, and (3) flashlight treatments. (d) Recording the effect of antibiofilm treatments with complementary readout of SECM and fluorescence microscopy.

2. Materials and Methods

2.1. Materials

FcMeOH (97%), silver nitrate (>99%), polyvinylpyrrolidone, ethylene glycol, and sodium azide were purchased from Sigma-Aldrich, Buchs, Switzerland. Phosphate-buffered saline (PBS, 10 mM, pH 7.4) was prepared with disodium phosphate (Na_2HPO_4 , 99.5%), monosodium phosphate (NaH_2PO_4 , 99.5%), and sodium chloride (NaCl , $\geq 99\%$), which were all bought from Sigma-Aldrich, Switzerland. Propidium iodide and SYTO™ 9 Green Fluorescent Nucleic Acid Stain were purchased from Thermo Fisher Scientific Company, Waltham, MA, USA. *E. coli* strain DH5 α was bought from Invitrogen, Waltham, MA, USA. All reagents and materials were of analytical grade and used as received. Deionized water was produced using a Milli-Q plus 185 model from Millipore, Zug, Switzerland.

2.2. Preparation of *E. coli* DH5 α Cell Cultures

E. coli strain DH5 α was grown as pre-cultures in LB at 37 °C for 6 h with continuous shaking at 200 rpm. Then, 100 μL of each pre-culture was added into 900 μL of 2xYT and incubated overnight at 37 °C with constant shaking at 150 rpm.

2.3. *E. coli* DH5 α Biofilm Culture

A total of 4 mL of 5 mM MgSO_4 in 2xYT was added to the solution of *E. coli* DH5 α cells (prepared in Section 2.2), which was incubated for 2 h under continuous shaking at 150 rpm. Glass slides were placed in the culture dish 60 (Thermo Fisher Scientific, Basel, Switzerland) and incubated overnight at 37 °C and 50% humidity. The biofilm formed at the interface between the glass substrate surface and air and/or culture medium. The presence of Mg^{2+} in the medium positively affected the initial attachment of bacterial cells, fostering biofilm formation [44] and increasing the biofilms' mechanical strengths [45].

2.4. Antibiotic Treatments for Biofilm Degradation

2.4.1. Sodium Azide

Sodium azide was prepared in 4 mM solution in DI water at room temperature. One-day-old biofilms on the glass slides were incubated at room temperature for 5 min and 15 min in the sodium azide-containing solution. After that, the sodium azide solution was washed away gently three times with DI water.

2.4.2. Silver Nanoparticles

Silver Nanoparticles Were Synthesized Using Three Different Methods

Synthesis 1. Silver nanoparticles were prepared by reducing dissolved silver nitrate using citrate. An aqueous solution of 17 mg of AgNO_3 in 100 mL water was heated under reflux and vigorous stirring for two minutes. After that, 10 mL of a 35 mM aqueous sodium citrate solution was rapidly added. The solution gradually turned yellow within a few minutes, indicating the formation of Ag nanoparticles. The solution was heated under reflux for 6 min. After that, the solution was cooled down to room temperature.

Synthesis 2. A 50 mg quantity of AgNO_3 (29.4 mmol) was first dissolved in 0.15 L deionized water, then 40 mL acetone was added and the resulting solution was mixed under magnetic agitation for 20 min. In this solution, 1.6 g PVP powder was added, and the agitation was continued for another 35 min. After 30 min stirring, PVP was observed to agglomerate and stick on the beaker's bottom and wall. The remaining acetone was decanted at the end of the mixing period. At the end of the experiment, the solid PVP (initially white) turned into a light brown and then a dark brown paste, indicating the formation of silver nanoparticles embedded in the polymer matrix. The final solid was then allowed to dry in the air for 48 h. The Ag/PVP colloid powder was dissolved in 50 mL water under magnetic agitation and kept stirring for 10 days, giving colloidal dispersions of PVP-protected silver in water [46].

Synthesis 3. In this synthesis, in the final steps, instead of dissolving in water (Synthesis 2), the Ag/PVP colloid was dissolved in 50 mL ethylene glycol to make a colloidal dispersion of PVP-protected silver in ethylene glycol for 10 days [46].

Reactions of AgNPs with Biofilms

For this process, $0.1 \mu\text{g}\cdot\text{mL}^{-1}$ and $1 \mu\text{g}\cdot\text{mL}^{-1}$ of AgNPs were added to the one-day-old biofilms on the glass slides and incubated at 37°C with 50% humidity for one day. Afterward, the sample was thoroughly rinsed with water three times to wash away the silver nanoparticles.

For both azide and silver treatments, the samples were air-dried and were used for complementary detections of live/dead fluorescence microscopy measurements and soft-probe-SECM.

The antimicrobial agents (sodium azide and silver nanoparticles) were dried using heat at 160°C for three hours before application to the biofilm.

2.4.3. Flashlight Irradiation for Treating Biofilms

The PulseForge 1300 photonic curing system (Novacentrix, Austin, TX, USA) was utilized to irradiate biofilms. Flashlight irradiation has been performed with a Xenon flashlight by pre-charging the capacitors of the lamp control units at 550 V for one, three, and five consecutive shots.

2.5. Confocal Laser Scanning Microscopy (CLSM) for Biofilm Characterization

CLSM was applied for biofilm studies. A 20 μM solution of SYTO 9 was prepared from a 5 mM stock solution in DMSO via dilution with PBS. Then, 300 μL of the solution was dropped on a biofilm-coated glass coverslip and incubated for 30 min at room temperature. The absorption wavelength and emission wavelength of SYTO 9 were 485 nm and 500 nm, respectively. Then, a 500 nM solution of PI was prepared by diluting a 1 mg/mL 1.5 mM stock solution in LB, and 300 μL of the solution was dropped on the biofilm-coated glass

coverslip and incubated for 5 min at room temperature. The absorption and emission wavelengths of PI were 535 nm and 617 nm, respectively. The Leica TCS SP8 white light laser (WLL) confocal microscope was used to visualize fluorescent markers.

2.6. Crystal Violet Staining of Biofilms

Biofilm-coated glass coverslips were washed three times with PBS and then dried at 60 °C for 15 min. Afterward, the coverslips were incubated in 2 mL of 0.1 wt% crystal violet staining solution for 15 min. Then, the coverslips were washed with PBS three times and dried at 60 °C for 15 min. After that, the stained biofilm was immersed in 30% acetic acid for 15 min to detach the stained biofilm from the glass slide. The solution was then analyzed with a Lambda 950S UV-Vis spectrophotometer (PerkinElmer, Waltham, MA, USA), and the results were given as optical density at 630 nm (OD_{630}).

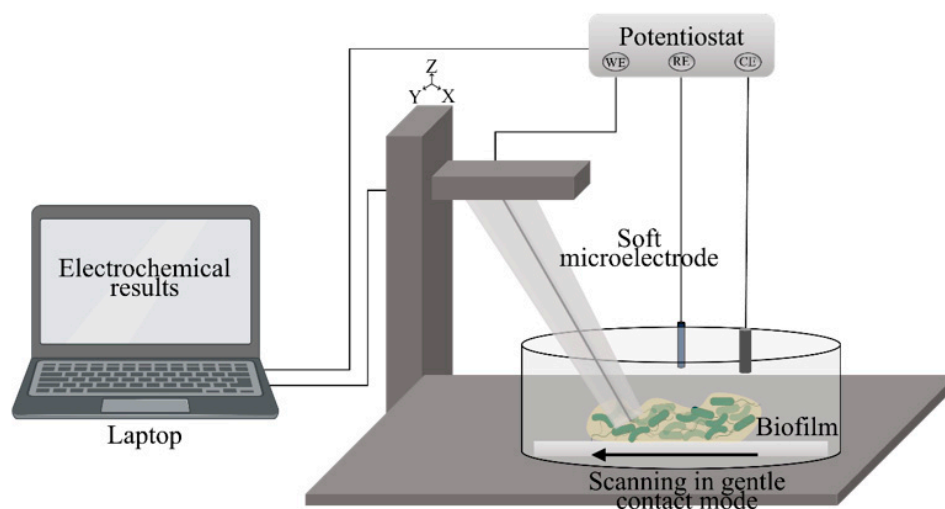
2.7. Characterization of AgNPs and Ag/PVP Nanocomposites

The synthesized AgNPs and Ag/PVP nanocomposites were characterized by using ultraviolet-visible spectroscopy (UV/Vis) (Lambda 950S UV-Vis spectrophotometer (PerkinElmer, Waltham, MA, USA)). Colloidal Ag/PVP of 0.05 mL was added to 5 mL water in a quartz cell. For Syntheses 1 and 2, the blank test was the corresponding water-PVP solution. In the case of ethylene glycol (Synthesis 3), the blank solution was the corresponding ethylene glycol-PVP solution, and the chosen volume was the same as the sample preparation for Syntheses 1 and 2.

Furthermore, AgNPs and nanocomposites' sizes were measured using dynamic light scattering (DLS) (Nano series, Malvern, UK), scanning electron microscopy (SEM), materials analysis with an X-ray detector for elemental mapping using X-ray energy-dispersive spectrometry (XEDS) (Dual-beam FEI Quanta, Corvallis, OR, USA), and atomic force microscopy (Dimension Icon with ScanAsyst from Bruker with tapping mode in air-standard).

2.8. Soft-Probe-SECM Measurements for Biofilm Study

SECM measurements were carried out in a three-electrode configuration using a home-made SECM setup running under SECMx software (G. Wittstock, University of Oldenburg) and comprising an Ivium Compactstat (Ivium Technologies, Eindhoven, Netherland) (Scheme 2). A soft SECM probe containing a carbon paste microelectrode (ME, active electrode area $\sim 100 \mu\text{m}^2$) acted as a working electrode, a silver wire was used as a quasi-reference electrode (QRE), and a platinum wire as a counter electrode (CE). All potentials noted herein for SECM measurements were referred to the QRE. The soft SECM probe (VersaScan (VS) Stylus probes obtained from Princeton Applied Research—Ametek, CA, USA) was made of a thin and flexible PET sheet of 100 μm thickness where the ME (electrode area $\sim 100 \mu\text{m}^2$) was embedded into a laser-drilled microchannel and sealed with a 2 μm thin Parylene C layer. Soft SECM probes were brushed over the samples in a gentle contact mode, with the Parylene C side touching the substrate. Prior to each experiment, the tip of the soft SECM probe was cut with a razor blade to provide a clean, active electrode surface. The probe was tilted by 20° with respect to the surface normal. All experiments were performed at room temperature (23 ± 2 °C). Lateral SECM probe translations were carried out with a working electrode potential $E_T = 0.5$ V for the oxidation of FcMeOH with probe translation speed = 25 $\mu\text{m}/\text{s}$, step size = 10 μm , and delay time between probe movement and current reading = 0.1 s. The experimental solution contained 2.5 mM FcMeOH in 100 mM PBS with pH 7.4.



Scheme 2. Schematic representing the SECM assembly used in the experiment.

3. Results and Discussion

3.1. SECM Investigation of Biofilm Degradation Induced with Azide

Herein, one-day-old *E. coli* biofilms were grown on a thin coverslip (the coverslip thickness was 170 μm) in a culture medium. The successful formation of the biofilm, i.e., viable and intact bacterial cells embedded in EPS, was confirmed using laser scanning microscopy, scanning electron microscopy (SEM, showing high-resolution images of the surface topography), and live/dead fluorescence microscopy (SI-1). The electron transfer chain of bacteria is located on the plasma membrane of the *E. coli* cells (Figure 1a) [47]. The redox mediator for SECM analysis must permeate through the outer membrane of the *E. coli* cells, reaching terminal metabolic redox enzymes of the electron transfer chain [48]. The outer leaflet of the outer membrane is composed of lipopolysaccharides (LPS), which are highly negatively charged and work as a selective permeability barrier [49]. One possibility for the transfer of the redox mediator is beta-barrel proteins, such as porins located in the outer membrane [50]. Porins are narrow channels that allow selective diffusion, driven by the concentration gradient between the two sides of the membrane. Porins allow, by passive diffusion, the passage of hydrophilic and lipophilic ions and molecules with molecular weights below 600 Da. Furthermore, lipophilic compounds may also cross the membranes directly [51,52]. The reduced form of the redox mediator must leave the bacterial cells through the outer membrane.

Soft-Probe-SECM in feedback mode was carried out in 100 mM PBS (pH 7.4) using 2.5 mM FcMeOH as a redox mediator for reading out the surface reactivity of the *E. coli* biofilm. By applying 0.5 V to the SECM probe, the oxidized forms of the redox mediator, positively charged FcMeOH^+ , were continuously generated and diffused towards the nearby biofilm. FcMeOH^+ , with a standard redox potential of 0.44 V [53], competed with O_2 as an electron acceptor. The inhibition of the respiratory chain affects the viability of *E. coli* cells through the proton motive force and electron transport chain [32,33], thus reducing FcMeOH^+ . During approach curves, the soft probe was tilted at an angle of 20° from the normal surface and controlled by the SECM probe holder. Once the probe touched the substrate surface, the SECM probe bent slightly on the plastic while the SECM current remained nearly constant, demonstrating the constant working distance. The probe was then pressed against the substrate by moving the SECM probe holder further downwards to reach a probe height of $-35 \mu\text{m}$. The probe height generally ranged from $-25 \mu\text{m}$ to $-35 \mu\text{m}$, and was applied and adjusted as needed to ensure that the soft probe was always in contact with the sample during line scan experiments.

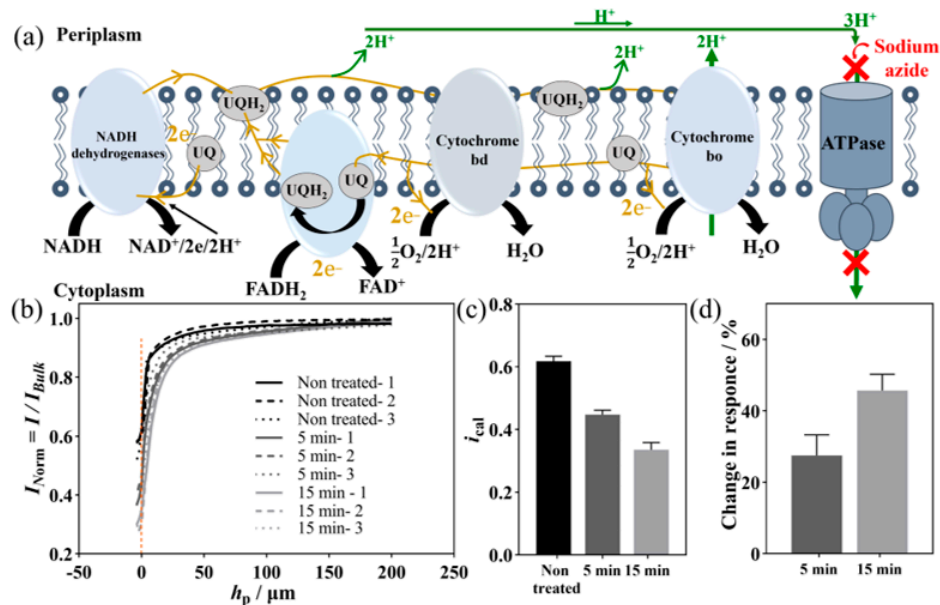


Figure 1. (a) Schematic representation of the respiratory electron transport chain in *E. coli*, including possible sites of electron transfer on the plasma membrane (adapted from Ref [46]). Dark yellow and green lines indicate the transfer paths of electrons and protons within the electron transport chain, respectively. (b) Soft-Probe-SECM approach curves for detecting the effect of azide treatment with incubation times of 5 and 15 min on *E. coli* biofilm on a glass coverslip (c) Mean \pm standard deviation of current at the touching point on the substrates. (d) Percentage of reduction in feedback current after 5 min and 15 min compared to the non-treated condition. Experimental details for approach curve SECM scans: working potential $E_T = 0.5$ V, probe translation speed = $5 \mu\text{m s}^{-1}$, step size = $2 \mu\text{m}$, 2.5 mM FcMeOH in 100 mM PBS (pH 7.4).

First, sodium azide was used to inhibit the metabolic activity of an *E. coli* biofilm. In metabolically active bacteria, ATPase in the plasma membrane catalyzes the synthesis of ATP from ADP (Figure 1a). This oxidative phosphorylation reaction is coupled to the proton motive force and proton transport from the outside of the bacterial cells into the cytoplasm [54]. Electron transfer reactions maintain the proton motive force (and thus the membrane potential). NADH serves as an electron donor, and its oxidation with NADH dehydrogenase pumps protons out of the cytoplasm. Under aerobic conditions, oxygen is the final electron acceptor. This results in the transport of up to eight protons [55]. The ETC comprises membrane-bound cytochromes (a-, b-, d-, o-type), dehydrogenases, quinones, and flavins. The sites of electron transfer of the anodic electron transport are cytochrome bo, cytochrome bd, Ubiquinone-pool, FAD reduction, and NADH oxidation, according to Equations (1)–(3) (Figure S3, E^0 given at 25 °C and pH 7 [55]):



The reported potentials (ox/red) of cytochromes a-, b-, d-, and o-type are 0.290 V, 0.080 V, 0.024 V, and 0.200 V, respectively [55]. In the aerobic respiration of *E. coli*, oxygen ($E^0 = 0.82$ V) acts as an electron acceptor [55].

Biofilms on a coverslip were incubated in a solution with 4 mM sodium azide, a potent inhibitor of bacterial growth [56]. Sodium azide inhibits bacterial growth by inhibiting the activity of SecA, an ATPase required to translocate proteins across the cytoplasmic membrane [57]. The inhibition of the three F1-ATPase catalytic sites was discussed in the

literature [58]. Three biofilms were grown on the coverslip and incubated in a sodium azide-containing solution. The same biofilms were evaluated for the non-treated samples. Three SECM approach curves were performed over the biofilms before and after incubation in sodium azide, each time followed by changing the solution and washing the biofilm. SECM measurements were carried out without antimicrobial agents. The details of SECM approach curve signals are presented in Table S1 and shown in Figure 1b. The average of the normalized currents over nontreated samples was (0.62 ± 0.02) , and after 5 min and 15 min it decreased to (0.45 ± 0.01) and (0.34 ± 0.02) for three different samples (Figure 1c). The feedback current decreased by 27% and 46%, respectively, after 5 min and 15 min incubation in sodium azide (Figure 1d). As the results show, the developed SECM approach is very sensitive to the effect of sodium azide treatment. It can record a significant change in the SECM current after 5 min of azide incubation. This may result from the reduced electron transport chain activity to reduce FcMeOH^+ and a reduced number of living bacterial cells. Therefore, with the feedback mode of SECM, the effect of ETC inhibitors on biofilms could be recorded quickly and with high sensitivity.

Furthermore, four SECM feedback line scans were performed, with a lateral space of 250 μm between them, on the same sample (Table S2 and Figure S4), and the mean calibrated current values for each line scan are shown in the bar plot in Figure S4d. The averages of the calibrated current over nontreated samples were (0.58 ± 0.004) , and after 5 min and 15 min they were (0.41 ± 0.003) and (0.33 ± 0.004) , respectively, for four different locations. The calibrated feedback current decreased by about 30% and 44% after incubation in sodium azide-containing solution for 5 min and 15 min. Therefore, the biofilm activity to reduce FcMeOH^+ upon inhibiting cellular respiration by sodium azide was reduced.

Furthermore, the inhibitory effect of sodium azide was evaluated with live/dead staining confocal laser scanning microscopy (CLSM). The effect of sodium azide treatment on the intact biomass of the biofilm was investigated with Cristal Violet (CV) staining. Before sodium azide treatment, as it is shown in Figure 2(ai,bi,ci), the biofilm mainly emitted a green color (both dead and living bacterial cells) and very few red colors (dead cells), indicating that the bacteria within the biofilm were predominantly alive. Figure 2d shows the biofilm biomass (i) before and after (ii) 5 min and (iii) 15 min incubation in sodium azide-containing solution.

The intensity values are presented in Table S3 and Figure 2e–g. The intensity of SYTO 9 staining was similar between the non-treated and azide-treated biofilms for the short incubation time, and it decreased by 9% after 5 min incubation. Furthermore, the biomass of the biofilm decreased by 6%. Both small changes in the intensity of SYTO 9 and CV suggest that the biofilm's total biomass was stable after 5 min. The changes in the intensity of SYTO 9 and CV after 15 min were 21% and 21%, respectively. The intensity of the red color emitted by the biofilms increased by 13% and 67% after 5 min and 15 min, indicating an increasing number of dead bacteria within the biofilm, with a particular impact after 15 min. As the results suggest, the optical microscopy techniques seemed to detect the effect of sodium azide over a long time with less sensitivity than SECM. Furthermore, biomass loss has been observed, mainly from washing the dyes essential for staining the biofilm. In the other study, Rapp et al. [59] used sodium azide as a biocide agent for monitoring biofilm destabilization and deactivation effects in real time. They treated *P.aeruginosa* biofilm with 1% *v/v* sodium azide solution and observed the impact of the treatment via continuous amperometric monitoring. They reported that the biofilm's respiratory activity was significantly impaired, and most of the bacteria within the biofilm were dead.

The statistical analysis of the results from live/dead fluorescence microscopy and SECM shows that the SECM readout is more sensitive for detecting the harsh effect of azide treatment than PI staining, which did not show a significant impact in a short time. PI is a membrane-impermeable dye generally used to distinguish intact from damaged cells. Sodium azide has the main inhibitory effect on the respiratory chain, and from the investigations herein, it is more readable with the feedback mode of SECM. Furthermore, as the previous study [59] shows, Soft-Probe-SECM appears sensitive to surface reactivity.

Therefore, even though washing the antimicrobial agents has a minor effect on biomass, it does not interfere with the SECM results. Furthermore, washing steps in the staining protocols lead to the removal of biomass, which has prominent external effects on the intensity of the images after treatments. As this result shows, after just 15 min, the biomass decreased by about 21% after sodium azide treatment and washing steps. Also, SECM could be recorded right after treating the biofilm and washing away the sodium azide since it does not need any treatment; however, for CLSM, sample preparation and staining steps are required.

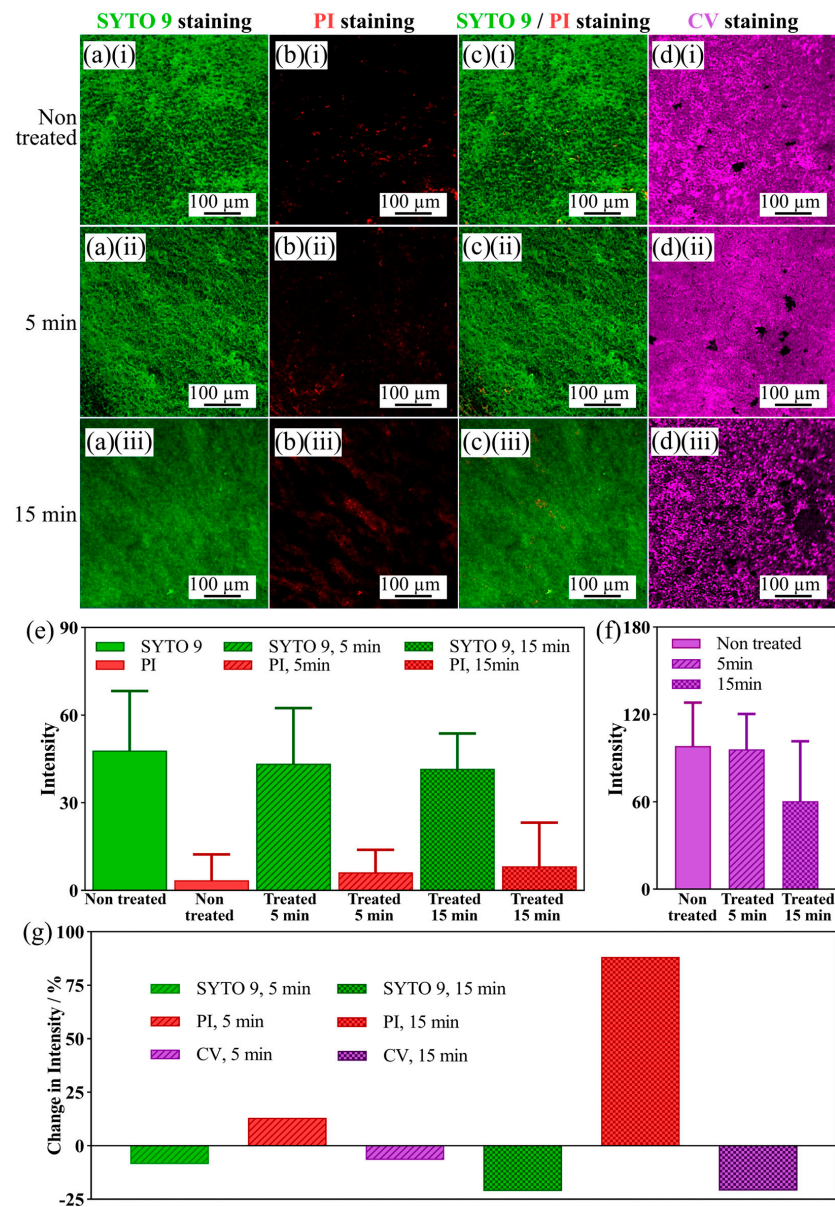


Figure 2. Live/dead co-staining of *E. coli* biofilm with (a) SYTO 9/(b) PI, and overlap of staining (c). (d) Biomass staining was performed with crystal violet staining. (i) Fluorescence image of biofilm before azide treatment. Fluorescence image of biofilm after (ii) 5 min and (iii) 15 min incubation in a solution with 10 mM sodium azide. Analysis of intensity from live/dead co-staining and biomass staining of *E. coli* biofilm with SYTO 9/PI and CV. (e) Bar plot of mean \pm standard deviation of the intensity of images in (a,b) calculated using ImageJ 1.53t. (f) Bar plot of mean \pm standard deviation of the intensity of images in (d) calculated using ImageJ. (g) Percentage of intensity changes compared to non-treated samples after different sodium azide incubation times.

3.2. SECM Investigation of Biofilm Degradation by Silver Nanoparticles

Silver nanoparticles (AgNPs) are widely used as antimicrobial agents [60]. The antibacterial activity of AgNPs is mainly associated with the generation of silver ions (Figure 3a). For instance, Ag(I) ions can interact with thiol groups on the cell surface, leading to the proton motive force collapse and, eventually, cell death [61]. Ag(I) ions (ionic radius of 0.115 nm) pass through porin channels (pore size, 1–3 nm) [60]. They can bind to membrane-bound enzymes and proteins containing thiol groups [62], interfere with DNA replication, and deactivate many enzymatic functions [60]. Ag(I) ions further increase the level of reactive oxygen species (ROS) inside the cell [63]. Moreover, AgNPs can mechanically create pores in the outer membrane, inducing physical damage to the bacterial cells. The mechanism of action of silver is linked to its interaction with thiol group compounds found in the respiratory enzymes of bacterial cells. Silver binds to the bacterial cell wall and cell membrane and inhibits respiration in the case of [64]. Silver acts by inhibiting phosphate uptake and releasing phosphate, mannitol, succinate, proline, and glutamine from *E. coli* cells [65]. The nanoparticles preferably attack the respiratory chain, causing cell division, finally leading to cell death. Herein, three different silver nanoparticles were synthesized. Citrate-capped AgNPs and Ag/PVP nanocomposites capped by PVP in water and ethylene glycol were successfully synthesized using a solution chemistry method (Figure 3b). The UV/Vis absorption spectra of AgNPs are shown in Figure S5a–c. The maximum absorption results of the studied nanocomposites were found at 473 nm, 442 nm, and 414 nm for citrate-capped AgNPs, PVP-capped AgNPs in water, and PVP-capped AgNPs in EG, respectively [55,66]. It has been reported that the absorption spectrum of spherical silver nanoparticles showed a maximum between 400 nm and 500 nm with a blue or red shift when the particle size diminished or increased, respectively [67,68]. Due to this reason, the nanocomposites synthesized in ethylene glycol showed a plasmon, which was blue shifted. AgNP size distributions determined by dynamic light scattering (DLS) and atomic force microscopy (AFM) are included in Figure 3c–h. AgNPs showed a single peak of hydrodynamic diameter distribution with the average peak in the number-weighted distribution at (23 ± 4) nm, (8 ± 2) nm, and (4 ± 1) nm for citrate-capped AgNP, PVP-capped AgNP in water, and EG. The single peaks obtained indicated the homogeneity of the particles' size. AFM results shown in Figure 3f–h confirmed the data from DLS. Further AgNPs analysis was conducted with SEM and Energy-dispersive X-ray spectroscopy (EDX) elemental mapping (SI-4).

Further intensity-weighted distributions are shown in Figure S5. The difference between intensity- and number-weighted distribution indicates that the initial suspension contained a fraction of aggregate particles that could not be thoroughly dispersed. The biofilm was incubated for 24 h in AgNP suspension. DLS was performed after 24 h (without dispersion and ultrasonication to simulate biofilm incubation over 24 h in a static environment). As shown in Figure 3f–h, after 24 h incubation, the number-weighted hydrodynamic diameter peak shifted to the larger particle size, indicating a substantial aggregation of primary particles. Citrate-capped AgNPs had shown a higher peak shift, indicating that PVP-capped AgNPs aggregated less. The PVP-capped AgNPs maintained their stability when incubated for 24 h, as indicated by stable DLS size distribution. Therefore, the important observation is that in contrast to citrate-capped AgNPs, after 24 h, PVP-capped AgNPs remained suspended, and these suspended particles were mostly unaggregated.

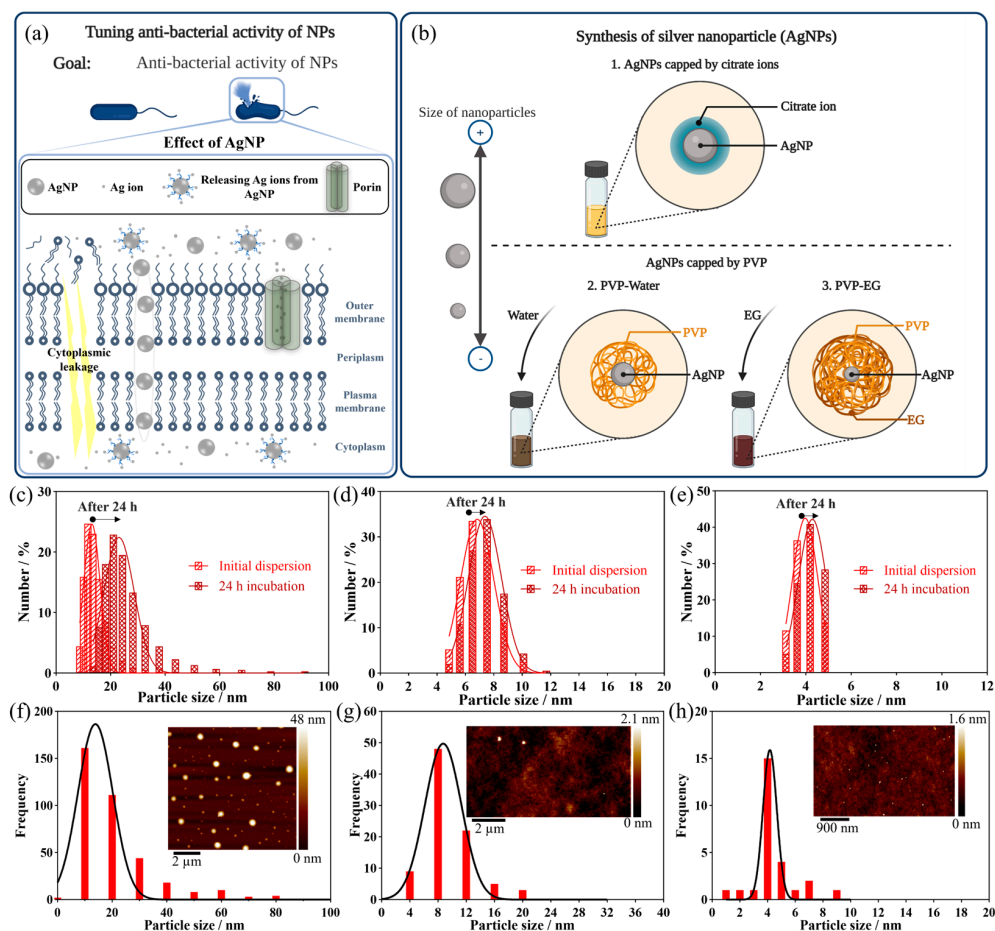


Figure 3. Treating biofilm with AgNPs: (a) schematic representing the effect of AgNPs against *E. coli*. (b) Synthesis of different AgNPs. Dynamic light scattering results of (c) citrate-capped AgNPs, PVP-capped AgNPs in water (d), and EG (e) based on the percentage of the count of number distribution. AFM of (f) AgNPs capped with citrate, PVP-capped AgNPs in (g) water, and (h) EG just after synthesis (insets are AFM maps.).

For SECM analysis, an *E. coli* biofilm was grown for one day on a coverslip and then partially covered with AgNPs for one additional day. Biofilms were exposed for one day to $0.1 \mu\text{g}\cdot\text{mL}^{-1}$ AgNP suspension, the minimum inhibitory concentration (MIC) of AgNP suspension for *E. coli* biofilm [69], and $1 \mu\text{g}\cdot\text{mL}^{-1}$ AgNO_3 , 10-fold that of MIC. The MIC of the AgNP suspension for biofilm was about 10 times higher than the MIC of planktonic bacteria due to the known enhanced resistance of the biofilm against antimicrobial reagents [69]. The AgNP suspension ($0.1 \mu\text{g}\cdot\text{mL}^{-1}$ and $1 \mu\text{g}\cdot\text{mL}^{-1}$ of AgNPs, $10 \mu\text{L}$) was dropped carefully on a small sample region only. This region appeared greyish and was, therefore, easy to locate with the naked eye. After the treatment, the solution and the AgNPs were gently but thoroughly washed away from the biofilm. Soft-Probe-SECM feedback z-line scanning (approach curves) of the treated and non-treated areas was performed for all three different AgNPs and for the two concentrations of AgNO_3 (MIC and 10 MIC) in triplicate with $250 \mu\text{m}$ lateral distance, and is shown in Figure 4.

Table S4 includes the normalized currents when the soft probe contacted the sample surface. The average of the normalized SECM currents is indicated in Table S5. The feedback current decreased about 24%, 32%, and 72% for $0.1 \mu\text{g}\cdot\text{mL}^{-1}$ of AgNPs and 55%, 68%, and 90% for $1 \mu\text{g}\cdot\text{mL}^{-1}$ of AgNPs of citrate-capped AgNPs, PVP-capped AgNPs in water, and EG, respectively (Figure 4). SECM results show that treated biofilms with Ag+ have lower feedback currents. This means that Ag+ treatment could damage the respiratory chain. Despite the effect of AgNPs on the electron transport chain, it has different effects,

e.g., a disruption of the cell membrane, the inactivation of proteins/enzymes, etc. This leads to a reduction in biofilm activity, specifically the respiration of the bacterial cells in the biofilm, which affects the feedback current recorded by SECM. EPS could act as a barrier for antimicrobial transport into the biofilm and play a role in the biofilm's extraordinary antimicrobial tolerance [70]. The relatively large sizes of AgNPs, especially their aggregates, suggest that transport hindrance could play a role in biofilm tolerance. As a result, the PVP-capped AgNPs in EG showed a prominent inhibitory effect with an apparent dropping in the feedback SECM current. It had almost twice the effect compared to PVP-capped AgNPs in water. This could come from two reasons. First, PVP-capped AgNPs in EG are small enough to pass through porin channels and have significant inhibitory effects. Second, the capping agents could decrease the interaction of AgNPs with the outer membrane. Therefore, PVP for the larger AgNPs could behave as a barrier and decrease the interaction while they are located outside of bacteria cells [67]. Hindered nanoparticle diffusion in biofilms has been demonstrated by Peulen and Wilkinson [71]. They observed a negligible diffusion of carboxylated polymer nanoparticles with diameters greater than 50 nm in laboratory-grown *P. fluorescens* biofilms with a reported thickness of less than 30 μm . In another study, Bard and co-workers [21] discussed the interaction of Ag^+ with the enzymes of the respiratory chain of *E. coli*. The authors suggested an inhibitory effect of Ag^+ at a low potential point, possibly by NADH dehydrogenase. Ferricyanide was used as an alternative electron acceptor to oxygen so that the reduction of ferricyanide to ferrocyanide by the respiration of *E. coli* was electrochemically followed. Ferricyanide is a hydrophilic molecule that does not pass the outer membrane to reach the plasma membrane. Therefore, the authors suggested the interaction of ferricyanide with a membrane-spanning protein, such as complex I or III, at some point in the periplasmic space, outside the cytoplasmic membrane [72]. Furthermore, the live/dead and biomass stainings have been investigated as complementary detection methods. PVP-capped AgNPs in EG ($1 \mu\text{g}\cdot\text{mL}^{-1}$ of AgNPs) were considered for biofilm treatment. Figure 5 shows the fluorescence images of two-day-old biofilm, including one day of growth in the solution with AgNPs, and details of the intensity of the figures were measured by ImageJ and were written in Table S6. The control was one-day-old biofilms (the same biofilm before treatment) without exposure to the AgNPs solution, demonstrating the bacterial cells' viability embedded in the non-treated biofilm (Figure 5a–d). As seen from the live/dead stained fluorescence images and biomass staining (Figure 5e–h), most bacteria died, and the intensity of PI staining (Figure 5i,j) increased by 90%. Furthermore, the biomass (Figure 5k) decreased by about 57%, indicating that the silver treatments also led to biofilm eradication. The previous study [51] reported that surface reactivity is most likely recorded with an SECM experiment. The recorded results of SECM and CLSM were quite similar, in contrast to the azide treatment discussed above. SECM showed a 90% reduction in feedback current, and CLSM showed a 90% increase in PI intensity. However, recording SECM approach curves is much faster than recording CLSM images. In this study, each approach curve took 50 sec; however, each CLSM image took more than 45 min, since the biofilm was about 12 μm thick and z-stacking imaging takes a long time.

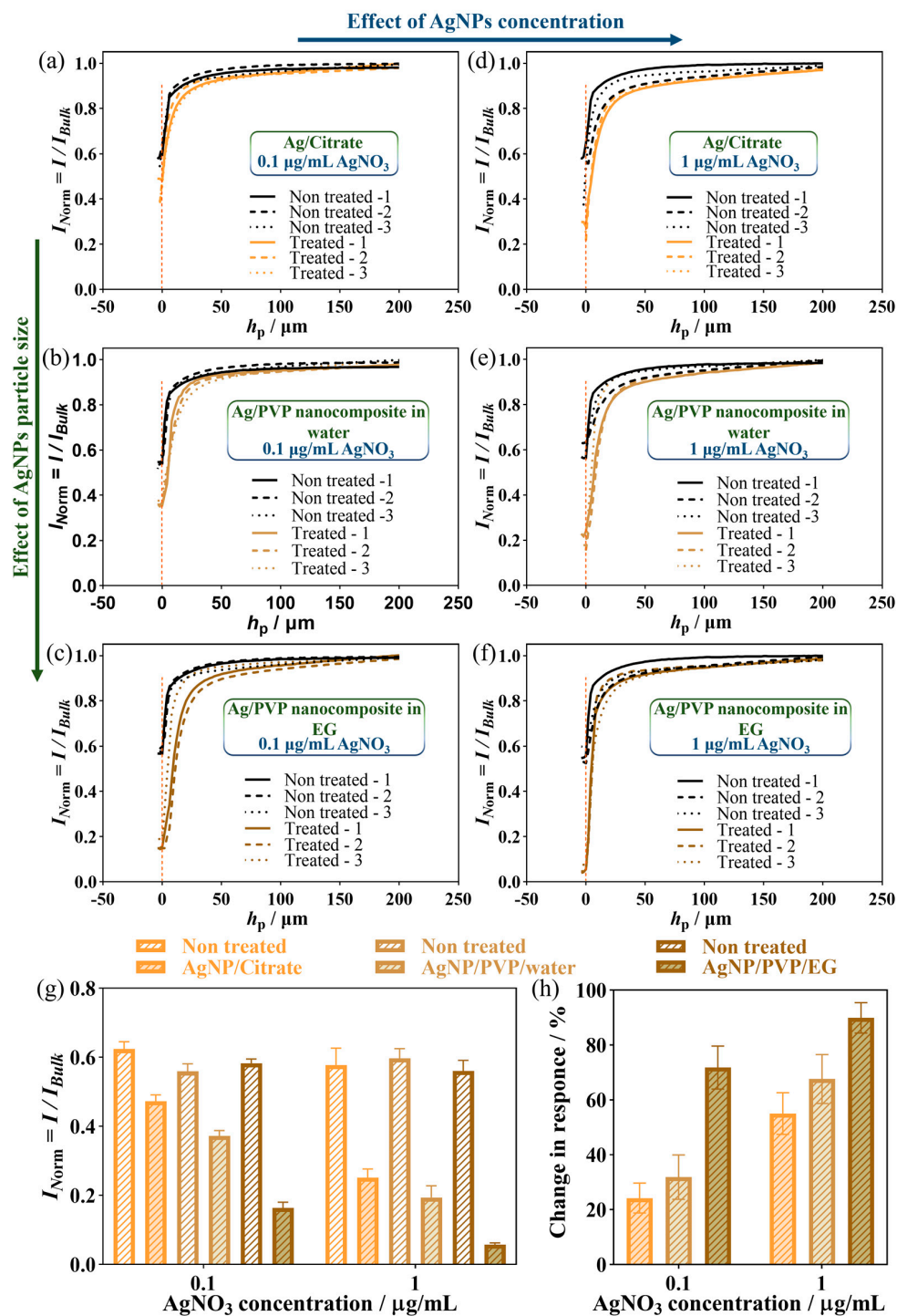


Figure 4. Soft-Probe-SECM approach curves for detecting the effect of AgNP on *E. coli* biofilm on a glass coverslip: treating one-day-old *E. coli* biofilm with 0.1 μg/mL AgNO₃ (a–c) and 1 μg/mL AgNO₃ (d–f). (a,d) *E. coli* biofilms were treated with citrate-capped AgNPs. (b,e) *E. coli* biofilms were treated with PVP-capped AgNPs in water. (c,f) *E. coli* biofilm was treated with PVP-capped AgNPs in EG. For each experiment, three different samples were evaluated. (g) Mean ± standard deviation of the normalized SECM current when the soft probe contacted the biofilm surface during approach curves. (h) Relative changes in the current response with respect to the non-treated sample. Experimental details for SECM approach curves: working potential $E_T = 0.5$ V, probe translation speed = 5 μm/s, step size = 2 μm, 2.5 mM FcMeOH in 100 mM PBS (pH 7.4).

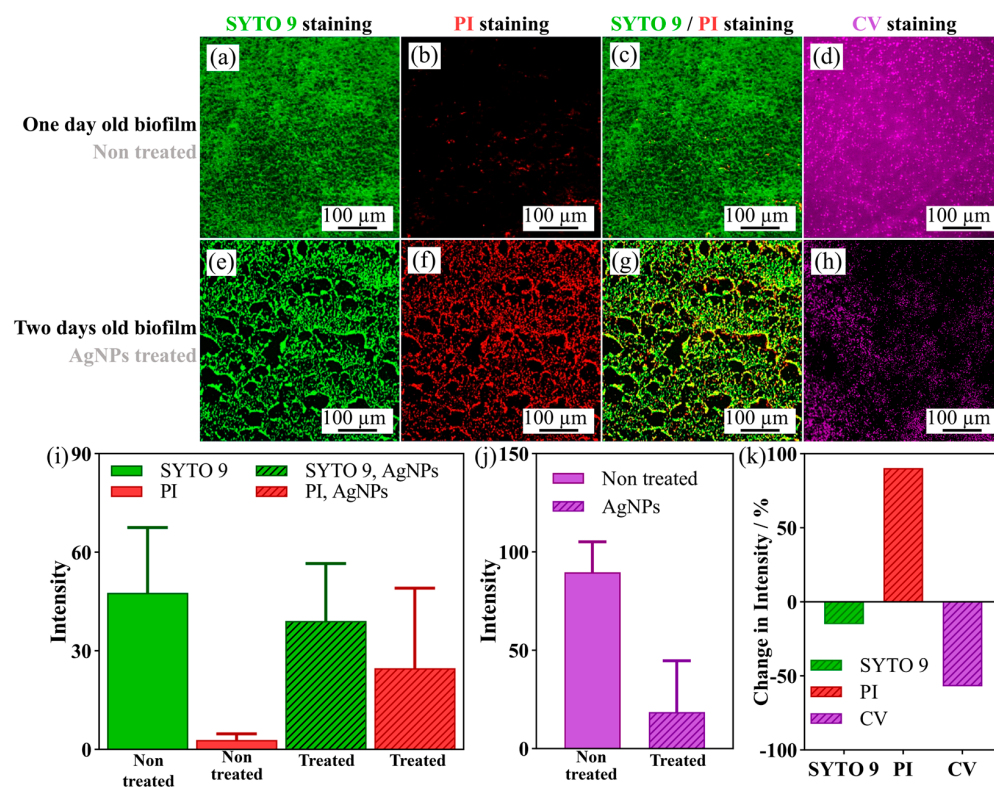


Figure 5. Fluorescence images of co-live/dead staining of SYTO 9/PI and biomass biofilm staining with CV. One-day-old biofilm was treated for one day with 1 $\mu\text{g}/\text{mL}$ AgNO_3 , which was synthesized with PVP-capped AgNPs in EG. (a) SYTO 9, (b) PI, (c) overlap of SYTO 9/PI, and (d) CV staining of non-treated sample. (e) SYTO 9, (f) PI, (g) overlap of SYTO 9/PI, and (h) CV staining of a treated sample after one-day incubation of one-day-old *E. coli* biofilm in AgNPs. (i) Mean intensity \pm standard deviation of the live/dead fluorescence image intensity was obtained from ImageJ for the non-treated and treated *E. coli* biofilm. (j) Mean intensity \pm standard deviation of the intensity of CV fluorescence images was obtained from ImageJ for the non-treated and treated biofilm. (k) Changes in intensity of the treated sample compared to the non-treated sample.

3.3. SECM Investigation of Biofilm Treatment by Flashlight

Lastly, the biofilm was treated with flashlight irradiation. The method uses a high-intensity Xe flash lamp whose emissions contain UV and white light (wavelengths from 200 nm to 1500 nm). As bacterial cells are prone to damage when exposed to UV light, rapid flashes might be used to disinfect environmental (water pipes) or clinical surfaces (operation equipment). The intensity of the flashlight is relatively high, reaching several J/cm^2 in a single flash. The flashlight irradiation technique is conducted at room temperature and air, thus under ambient conditions [70]. Herein, a one-day-old *E. coli* biofilm was treated with flashlight irradiation, applying 550 V for charging the lamp driving capacitors for different numbers of shots, i.e., one, three, and five. Figure 6 shows the SECM feedback response of the flashlight-treated biofilms. Tables S7 and S8 indicate the details of the SECM currents at the contact point between the soft probe and the biofilm surface. The current decreased by 20%, 78%, and 88% after treating the biofilm with the 550 V flashlight irradiation in one, three, and five shots.

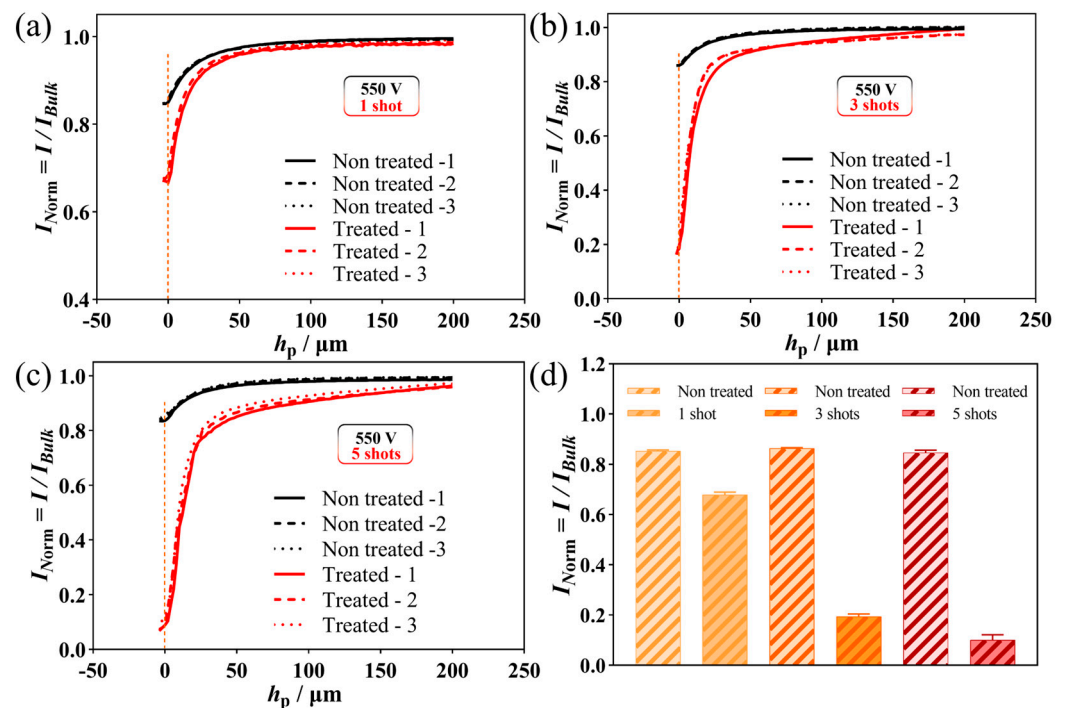


Figure 6. Soft-Probe-SECM approach curves of detection of the effect of flashlight on *E. coli* biofilm on the coverslip: treating one-day-old *E. coli* biofilm with (a) 550 V, 1 shot, (b) 550 V, 3 shots, and (c) 550 V, 5 shots of the flashlight. (d) Mean \pm standard deviation of SECM approach curves. Experimental details for approach curve SECM scans: working potential $E_T = 0.5$ V, probe translation speed = $5 \mu\text{m/s}$, step size = $2 \mu\text{m}$, 2.5 mM FcMeOH in 100 mM PBS (pH 7.4).

Complementary detection has been performed based on Co-SYTO 9/PI staining (Figure 7). As illustrated, the flashlight treatment killed the bacteria. Still, it also partially removed the biofilm, leading to biofilm eradication. The details of each fluorescence image with each fluorescence image's intensity were assessed using ImageJ and are indicated in Table S9. The intensity of PI staining increased by 21%, 63%, and 79% by treating the biofilm with the 550 V-driven flashlight using one, three, and five shots.

Flashlight irradiation is a quick and clean technique for treating biofilm. In a case in vivo, applications are envisaged whereby a large portion of UV with high intensity must be considered, and measures must be applied to enable a safe operation for the organs. However, flashlight treatments of biofilms could be considered a powerful biofilm eradication technique for environmental applications.

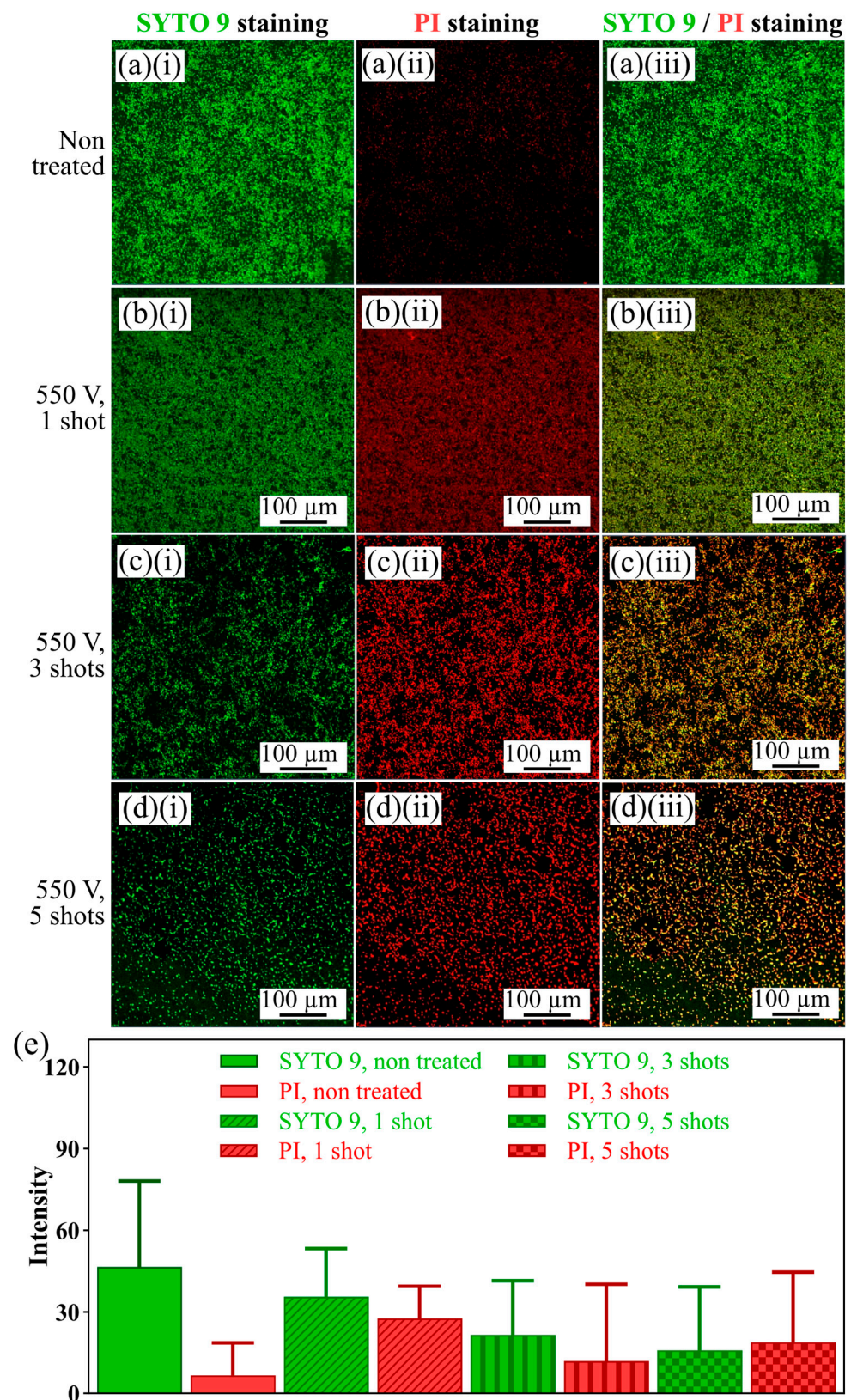


Figure 7. Fluorescence images of co-live/dead staining of SYTO 9/PI. (a) Non-treated sample. One-day-old biofilm was treated with flashlight in 550 V with one (b), three (c), and five shots (d). (i) SYTO 9 staining, (ii) PI staining, and (iii) co SYTO 9/PI staining. (e) Mean intensity ± standard deviation of the live/dead fluorescence image intensity was obtained from ImageJ for the non-treated and treated *E. coli* biofilm.

4. Conclusions

To conclude, Soft-Probe-SECM of *E. coli* biofilms treated with different antimicrobial agents and treatments are presented. The antimicrobial agents were sodium azide, a respiratory chain inhibitor, and silver nanoparticles, which disrupt cellular membranes, proteins, and polysaccharides. In addition, biofilms were treated with light flashes generated from a high-intensity Xenon flash lamp. The antimicrobial concentrations were 4 mM sodium azide and $0.1 \mu\text{g}\cdot\text{mL}^{-1}$ AgNO_3 and $1 \mu\text{g}\cdot\text{mL}^{-1}$ AgNO_3 , and the change in the biofilm properties was followed depending on the treatment time for sodium azide and the size of the nanoparticles for the silver nanoparticle treatment. The inhibitory effect of these agents on cell viability was confirmed by using live/dead fluorescence imaging and biomass staining. The SYTO 9 intensity indicated that the total number of living and dead bacterial cells remained constant, independent of the applied antimicrobial treatment. PI intensity showed an increasing number of dead bacterial cells with treatment. The SECM feedback mode was used, and feedback currents decreased after the biofilms were treated with antimicrobial strategies. The feedback current reduction was most likely recorded based on the surface reactivity of treated samples. SECM revealed a change in biofilm activity after only 5 min. Similarly, the feedback SECM current reduction after exposure to AgNPs was significant, suggesting that SECM could record the biocide effects of sodium azide on the electron transfer chain more sensitively than fluorescence microscopy at short treatment times. Furthermore, flashlight irradiation was used as a quick technique. The results indicated that this technique is a powerful tool for biofilm eradication. The results demonstrate that SECM could become a powerful technique for recording various agents' effects with an inhibitory effect at the intracellular level, especially those affecting the respiratory chain. SECM was very sensitive, with fast responses compared to the complementary techniques. SECM approach curves were recorded in less than a minute. Furthermore, SECM in the modes applied herein did not acquire any sample pre-treatment, as the sensitive marker was a redox mediator in the solution.

Supplementary Materials: The following supporting information can be downloaded at: <https://www.mdpi.com/article/10.3390/applnano4030015/s1>. Figure S1: Investigating the presence of one-day-old *E. coli* biofilm grown on a coverslip using microscopy: (a,b) laser scanning micrograph in two magnifications. (c,d) SEM images at three different magnifications. (e) Fluorescence crystal violet biomass staining. (f) Fluorescence images of SYTO 9/ PI co-staining. SYTO 9 (green color) stained all bacteria, and PI (red color) stained dead bacteria; Figure S2 (a) 3D structure of one-day-old *E. coli* biofilm on the coverslip. (b) Height profile of the biofilm. The color bar indicates the height of the biofilm; Figure S3: Redox potentials of important redox couples in the electron transport chain of *E. coli*. Standard redox potentials (E^0 [mV, 25 °C, pH 7]) are indicated. Physiological or environmental conditions are known to shift the potential from the E^0 , and redox windows are indicated [1]; Figure S4: X-line scans SECM in four separated positions with a lateral distance of 250 μm before sodium azide treatment (a), after 5 min (b), and after 15 min of sodium azide treatment. (d) Calibrated mean currents \pm standard deviation of three SECM feedback line scans over *E. coli* biofilm before and after 5 min and 15 min incubation of the biofilm in sodium azide-containing solution, grouped by (b) line scan position and (c) grouped by treatment time. Experimental details for x-line SECM scans: working potential $E_T = 0.5$ V, probe translation speed = $25 \mu\text{m s}^{-1}$, step size = $10 \mu\text{m}$, 2.5 mM FcMeOH in 100 mM PBS (pH 7.4); Figure S5: UV-Vis spectra of (a) AgNPs capped with citrate, PVP-capped AgNPs in (b) water, and (c) EG just after synthesis; Figure S6: (a) AFM map of citrate-capped AgNP and (b) plot of particle size distribution of citrate-capped AgNP; Figure S7: (a,b) AFM map of PVP-capped AgNP in water in two areas of sample and (c) plot of particle size distribution of citrate-capped AgNP; Figure S8: (a) AFM map of PVP-capped AgNP in EG and (b) plot of particle size distribution of citrate-capped AgNP; Figure S9: SEM images of (a) AgNPs capped with citrate, PVP-capped AgNPs in (b) water, and (c) EG; Figure S10: EDX elemental mapping of AgNPs capped with citrate: (a) SEM image. Elemental mapping of (b) Ag, (c) Si, (d) C, and (e) O. (f) EDX analysis; Figure S11: EDX elemental mapping of PVP-capped AgNPs in water: (a) SEM image. Elemental mapping of (b) Ag, (c) Si, (d) C, and (e) O. (f) EDX analysis; Figure S12: EDX elemental mapping of PVP-capped AgNPs in EG: (a) SEM image. Elemental mapping of (b) Ag,

(c) Si, (d) C, and (e) O. (f) EDX analysis; Table S1: details SECM currents at the contact point of the soft probe with the biofilm surface; Table S2: details the SECM x-line scan data of Figure S4; Table S3: Details about quantification intensity data of Figure 2.; Table S4: Details of SECM z-line scan data at the approached point of Figure 4. Table S5: Details of the average of SECM z-line scan data at the approached point of Table S4. N = sample number; Table S6: Details about quantification intensity data of Figure 5; Table S7: Details of SECM z-line scan data at the approached point of Figure 6; Table S8: Details of the average of SECM z-line scan data at the approached point of Table S7; Table S9 Details about quantification intensity data of Figure 7.

Author Contributions: Conceptualization, S.D.; methodology, S.D.; validation, S.D.; formal analysis, S.D.; investigation, S.D.; resources, H.H.G.; writing—original draft preparation, S.D.; writing—review and editing, S.D. and H.H.G.; supervision, H.H.G. All authors have read and agreed to the published version of the manuscript.

Funding: This research received no external funding.

Data Availability Statement: The data that support the findings of this study are available from the corresponding author, upon reasonable request.

Acknowledgments: S.D. acknowledges the support from the Swiss National Science Foundation Project No. P500PN_206581. We thank Andreas Lesch (University of Bologna) for his suggestions on the SECM readout and Horst Pick (Ecole Polytechnique Fédérale de Lausanne (EPFL)) for providing the primary source of the bacteria sample. Also, we appreciate the great data analysis from Setayesh Darvishi (Isfahan University of Technology).

Conflicts of Interest: The authors declare no conflict of interest.

References

1. Donlan, R.M. Biofilms: Microbial life on surfaces. *Emerg. Infect. Dis.* **2002**, *8*, 881–890. [[CrossRef](#)] [[PubMed](#)]
2. Koo, H.; Allan, R.N.; Howlin, R.P.; Stoodley, P.; Hall-Stoodley, L. Targeting microbial biofilms: Current and prospective therapeutic strategies. *Nat. Rev. Microbiol.* **2017**, *15*, 740–755. [[CrossRef](#)] [[PubMed](#)]
3. Ciofu, O.; Tolker-Nielsen, T. Tolerance and resistance of *Pseudomonas aeruginosa* biofilms to antimicrobial agents—How *P. aeruginosa* can escape antibiotics. *Front. Microbiol.* **2019**, *10*, 913–927. [[CrossRef](#)] [[PubMed](#)]
4. Nocker, A.; Camper, A.K. Novel approaches toward preferential detection of viable cells using nucleic acid amplification techniques. *EMS Microbiol. Lett.* **2009**, *291*, 137–142. [[CrossRef](#)]
5. Pettit, R.K.; Weber, C.A.; Kean, M.J.; Hoffmann, H.; Pettit, G.R.; Tan, R.; Franks, K.S.; Horton, M.L. Microplate Alamar blue assay for *Staphylococcus epidermidis* biofilm susceptibility testing. *Antimicrob. Agents Chemother.* **2005**, *49*, 2612–2617. [[CrossRef](#)]
6. Mariscal, A.; Lopez-Gigosos, R.M.; Carnero-Varo, M.; Fernandez-Crehuet, J. Fluorescent assay based on resazurin for detection of activity of disinfectants against bacterial biofilm. *Appl. Microbiol. Biotechnol.* **2009**, *82*, 773–783. [[CrossRef](#)]
7. Peeters, E.; Nelis, H.J.; Coenye, T. Comparison of multiple methods for quantification of microbial biofilms grown in microtiter plates. *J. Microbiol. Methods* **2008**, *72*, 157–165. [[CrossRef](#)]
8. Welch, K.; Cai, Y.; Strømme, M. A method for quantitative determination of biofilm viability. *J. Funct. Biomater.* **2012**, *3*, 418–431. [[CrossRef](#)]
9. Braissant, O.; Astasov-Frauenhoffer, M.; Waltimo, T.; Bonkat, G. A review of methods to determine viability, vitality, and metabolic rates in microbiology. *Front. Microbiol.* **2020**, *11*, 547458. [[CrossRef](#)]
10. Cesewski, E.; Johnson, B.N. Electrochemical biosensors for pathogen detection. *Biosens. Bioelectron.* **2020**, *159*, 112214. [[CrossRef](#)]
11. Darvishi, S.; Pick, H.; Lin, T.E.; Zhu, Y.; Li, X.; Ho, P.C.; Girault, H.H.; Lesch, A. Tape-stripping electrochemical detection of melanoma. *Anal. Chem.* **2019**, *91*, 12900–12908. [[CrossRef](#)]
12. Darvishi, S.; Souissi, M.; Karimzadeh, F.; Kharaziha, M.; Sahara, R.; Ahadian, S. Ni nanoparticle-decorated reduced graphene oxide for non-enzymatic glucose sensing: An experimental and modeling study. *Electrochim. Acta* **2017**, *240*, 388–398. [[CrossRef](#)]
13. Darvishi, S.; Souissi, M.; Kharaziha, M.; Karimzadeh, F.; Sahara, R.; Ahadian, S. Gelatin methacryloyl hydrogel for glucose biosensing using Ni nanoparticles-reduced graphene oxide: An experimental and modeling study. *Electrochim. Acta* **2018**, *261*, 275–283. [[CrossRef](#)]
14. Darvishi, S.; Karmizadeh, F.; Kharaziha, M. A facile one-step electrochemical synthesis of nickel nanoparticle/Graphene composites for non-enzymatic biosensor applications. *Procedia Mater. Sci.* **2015**, *11*, 142–146. [[CrossRef](#)]
15. Caniglia, G.; Kranz, C. Scanning electrochemical microscopy and its potential for studying biofilms and antimicrobial coatings. *Anal. Bioanal. Chem.* **2020**, *412*, 6133–6148. [[CrossRef](#)]
16. Abucayon, E.; Ke, N.; Cornut, R.; Patelunas, A.; Miller, D.; Nishiguchi, M.K.; Zoski, C.G. Investigating catalase activity through hydrogen peroxide decomposition by bacteria biofilms in real time using scanning electrochemical microscopy. *Anal. Chem.* **2014**, *86*, 498–505. [[CrossRef](#)]

17. Joshi, V.S.; Kreth, J.; Koley, D. Pt-decorated MWCNTs–ionic liquid composite-based hydrogen peroxide sensor to study microbial metabolism using scanning electrochemical microscopy. *Anal. Chem.* **2017**, *89*, 7709–7718. [[CrossRef](#)]
18. Connell, J.L.; Kim, J.; Shear, J.B.; Bard, A.J.; Whiteley, M. Real-time monitoring of quorum sensing in 3D-printed bacterial aggregates using scanning electrochemical microscopy. *Proc. Natl. Acad. Sci. USA* **2014**, *111*, 18255–18260. [[CrossRef](#)]
19. Koley, D.; Ramsey, M.M.; Bard, A.J.; Whiteley, M. Discovery of a biofilm electroline using real-time 3D metabolite analysis. *Proc. Natl. Acad. Sci. USA* **2011**, *108*, 19996–20001. [[CrossRef](#)]
20. Meirelles, L.A.; Newman, D.K. Both toxic and beneficial effects of pyocyanin contribute to the lifecycle of *Pseudomonas aeruginosa*. *Mol. Microbiol.* **2018**, *110*, 995–1010. [[CrossRef](#)]
21. Holt, K.B.; Bard, A.J. Interaction of silver (I) ions with the respiratory chain of *Escherichia coli*: An electrochemical and scanning electrochemical microscopy study of the antimicrobial mechanism of micromolar Ag⁺. *Biochemistry* **2005**, *44*, 13214–13223. [[CrossRef](#)]
22. Pecchiolan, G.; Battistel, D.; Daniele, S. Scanning Electrochemical Microscopy and Voltammetric Investigation of Silver Nanoparticles Embedded within a Nafion Membrane. *ChemElectroChem* **2016**, *3*, 2297–2304. [[CrossRef](#)]
23. Fan, F.-R.F.; Bard, A.J. Chemical, electrochemical, gravimetric, and microscopic studies on antimicrobial silver films. *J. Phys. Chem. B* **2002**, *106*, 279–287. [[CrossRef](#)]
24. Aponso, S.; Ummadi, J.G.; Davis, H.; Ferracane, J.; Koley, D. A chemical approach to optimizing bioactive glass dental composites. *J. Dent. Res.* **2019**, *98*, 194–199. [[CrossRef](#)] [[PubMed](#)]
25. Vidallon, M.L.P.; Teo, B.M. Recent developments in biomolecule-based nanoencapsulation systems for antimicrobial delivery and biofilm disruption. *Chem. Commun.* **2020**, *56*, 13907–13917. [[CrossRef](#)]
26. Li, X.; Wu, B.; Chen, H.; Nan, K.; Jin, Y.; Sun, L.; Wang, B. Recent developments in smart antibacterial surfaces to inhibit biofilm formation and bacterial infections. *J. Mater. Chem. B* **2018**, *6*, 4274–4292. [[CrossRef](#)]
27. Darvishi, S.; Tavakoli, S.; Kharaziha, M.; Girault, H.H.; Kaminski, C.F.; Mela, I. Advances in the Sensing and Treatment of Wound Biofilms. *Angew. Chem. Int. Ed.* **2022**, *61*, e202112218. [[CrossRef](#)]
28. Mohanta, Y.K.; Biswas, K.; Jena, S.K.; Hashem, A.; Abd_Allah, E.F.; Mohanta, T.K. Anti-biofilm and antibacterial activities of silver nanoparticles synthesized by the reducing activity of phytoconstituents present in the Indian medicinal plants. *Front. Microbiol.* **2020**, *11*, 1143. [[CrossRef](#)] [[PubMed](#)]
29. Xu, X.; Wang, Y.; Liao, S.; Wen, Z.T.; Fan, Y. Synthesis and characterization of antibacterial dental monomers and composites. *J. Biomed. Mater. Res.—B Appl. Biomater.* **2012**, *100*, 1151–1162. [[CrossRef](#)]
30. Lee, W.H.; Pressman, J.G.; Wahman, D.G. Three-dimensional free chlorine and monochloramine biofilm penetration: Correlating penetration with biofilm activity and viability. *Environ. Sci. Technol.* **2018**, *52*, 1889–1898. [[CrossRef](#)]
31. Leung, D.; Spratt, D.A.; Pratten, J.; Gulabivala, K.; Mordan, N.J.; Young, A.M. Chlorhexidine-releasing methacrylate dental composite materials. *Biomaterials* **2005**, *26*, 7145–7153. [[CrossRef](#)] [[PubMed](#)]
32. Cabrol, L.; Quemeneur, M.; Misson, B. Inhibitory effects of sodium azide on microbial growth in experimental resuspension of marine sediment. *J. Microbiol. Methods* **2017**, *133*, 62–65. [[CrossRef](#)] [[PubMed](#)]
33. Darvishi, S.; Pick, H.; Oveisi, E.; Girault, H.H.; Lesch, A. Soft-probe-scanning electrochemical microscopy reveals electrochemical surface reactivity of *E. coli* biofilms. *Sens. Actuators B Chem.* **2021**, *334*, 129669. [[CrossRef](#)]
34. Lawrence, C.; Waechter, S.; Alsanus, B.W. Blue Light Inhibits *E. coli*, but Decisive Parameters Remain Hidden in the Dark: Systematic Review and Meta-Analysis. *Front. Microbiol.* **2022**, *13*, 867865. [[CrossRef](#)]
35. Yuan, H.; Zhang, X.; Jiang, Z.; Wang, X.; Wang, Y.; Cao, L.; Zhang, X. Effect of light spectra on microalgal biofilm: Cell growth, photosynthetic property, and main organic composition. *Renew. Energy* **2020**, *157*, 83–89. [[CrossRef](#)]
36. Yin, R.; Dai, T.; Avci, P.; Jorge, A.E.S.; de Melo, W.C.; Vecchio, D.; Huang, Y.Y.; Gupta, A.; Hamblin, M.R. Light based anti-infectives: Ultraviolet C irradiation, photodynamic therapy, blue light, and beyond. *Curr. Opin. Pharmacol.* **2013**, *13*, 731–762. [[CrossRef](#)] [[PubMed](#)]
37. Wilson, M. Lethal photosensitisation of oral bacteria and its potential application in the photodynamic therapy of oral infections. *Photochem. Photobiol. Sci.* **2004**, *3*, 412–418. [[CrossRef](#)]
38. De Melo, W.C.; Avci, P.; De Oliveira, M.N.; Gupta, A.; Vecchio, D.; Sadasivam, M.; Chandran, R.; Huang, Y.Y.; Yin, R.; Perussi, L.R.; et al. Photodynamic inactivation of biofilm: Taking a lightly colored approach to stubborn infection. *Expert Rev. Anti-Infect. Ther.* **2013**, *11*, 669–693. [[CrossRef](#)]
39. El Najjar, N.; van Teeseling, M.C.; Mayer, B.; Hermann, S.; Thanbichler, M.; Graumann, P.L. Bacterial cell growth is arrested by violet and blue, but not yellow light excitation during fluorescence microscopy. *BMC Mol. Biol.* **2020**, *21*, 35. [[CrossRef](#)]
40. Rezaie, A.; Leite, G.G.; Melmed, G.Y.; Mathur, R.; Villanueva-Millan, M.J.; Parodi, G.; Sin, J.; Germano, J.F.; Morales, W.; Weitsman, S.; et al. Ultraviolet A light effectively reduces bacteria and viruses including coronavirus. *PLoS ONE* **2020**, *15*, e0236199. [[CrossRef](#)]
41. Pullerits, K.; Ahlinder, J.; Holmer, L.; Salomonsson, E.; Öhrman, C.; Jacobsson, K.; Dryselius, R.; Forsman, M.; Paul, C.J.; Rådström, P. Impact of UV irradiation at full scale on bacterial communities in drinking water. *NPJ Clean Water* **2020**, *3*, 11. [[CrossRef](#)]
42. Komerik, N.; MacRobert, A.J. Photodynamic therapy as an alternative antimicrobial modality for oral infections. *J. Environ. Pathol. Toxicol. Oncol.* **2006**, *25*, 487–504. [[CrossRef](#)]
43. Song, B.; Leff, L.G. Influence of magnesium ions on biofilm formation by *Pseudomonas fluorescens*. *Microbiol. Res.* **2006**, *161*, 355–361. [[CrossRef](#)]

44. Körstgens, V.; Flemming, H.-C.; Wingender, J.; Borchard, W. Influence of calcium ions on the mechanical properties of a model biofilm of mucoid *Pseudomonas aeruginosa*. *Water Sci. Technol.* **2001**, *43*, 49–57. [[CrossRef](#)] [[PubMed](#)]
45. Arshi, N.; Ahmed, F.; Kumar, S.; Anwar, M.; Koo, B.H.; Lee, C.G. Comparative study of the Ag/PVP nanocomposites synthesized in water and in ethylene glycol. *Curr. Appl. Phys.* **2011**, *11*, S346–S349. [[CrossRef](#)]
46. Silhavy, T.J.; Kahne, D.; Walker, S. The bacterial cell envelope. *Cold Spring Harb. Perspect. Biol.* **2010**, *2*, a000414. [[CrossRef](#)] [[PubMed](#)]
47. Chotinantakul, K.; Suginta, W.; Schulte, A. Advanced amperometric respiration assay for antimicrobial susceptibility testing. *Anal. Chem.* **2014**, *86*, 10315–10322. [[CrossRef](#)]
48. Nikaido, H. Molecular basis of bacterial outer membrane permeability revisited. *Microbiol. Mol. Biol. Rev.* **2003**, *67*, 593–656. [[CrossRef](#)]
49. Ruiz, N.; Kahne, D.; Silhavy, T.J. Advances in understanding bacterial outer-membrane biogenesis. *Nat. Rev. Microbiol.* **2006**, *4*, 57–66. [[CrossRef](#)]
50. Muheim, C.; Götzke, H.; Eriksson, A.U.; Lindberg, S.; Lauritsen, I.; Nørholm, M.H.; Daley, D.O. Increasing the permeability of *Escherichia coli* using MAC13243. *Sci. Rep.* **2017**, *7*, 17629–17639. [[CrossRef](#)]
51. Amro, N.A.; Kotra, L.P.; Wadu-Mesthrige, K.; Bulychev, A.; Mobashery, S.; Liu, G.-Y. High-resolution atomic force microscopy studies of the *Escherichia coli* outer membrane: Structural basis for permeability. *Langmuir* **2000**, *16*, 2789–2796. [[CrossRef](#)]
52. Mirkin, M.V.; Bard, A.J. *Scanning Electrochemical Microscopy*, 2nd ed.; CRC Press: Boca Raton, FL, USA, 2012. [[CrossRef](#)]
53. Miller, S.I.; Salama, N.R. The gram-negative bacterial periplasm: Size matters. *PLoS Biol.* **2018**, *16*, e2004935. [[CrossRef](#)] [[PubMed](#)]
54. Kracke, F.; Vassilev, I.; Krömer, J.O. Microbial electron transport and energy conservation—the foundation for optimizing bioelectrochemical systems. *Front. Microbiol.* **2015**, *6*, 575. [[CrossRef](#)] [[PubMed](#)]
55. Hamed, M.B.; Burchacka, E.; Angus, L.; Marchand, A.; De Geyter, J.; Loos, M.S.; Anné, J.; Klaassen, H.; Chaltin, P.; Karamanou, S.; et al. Effective Small Molecule Antibacterials from a Novel Anti-Protein Secretion Screen. *Microorganisms* **2021**, *9*, 592. [[CrossRef](#)]
56. Oliver, D.B.; Cabelli, R.J.; Dolan, K.M.; Jarosik, G.P. Azide-resistant mutants of *Escherichia coli* alter the SecA protein, an azide-sensitive component of the protein export machinery. *Proc. Natl. Acad. Sci. USA* **1990**, *87*, 8227–8231. [[CrossRef](#)] [[PubMed](#)]
57. Weber, J.; Senior, A.E. Effects of the inhibitors azide, dicyclohexylcarbodiimide, and aurovertin on nucleotide binding to the three F1-ATPase catalytic sites measured using specific tryptophan probes. *J. Biol. Chem.* **1998**, *273*, 33210–33215. [[CrossRef](#)]
58. Pires, L.; Sachsenheimer, K.; Kleintschek, T.; Waldbaur, A.; Schwartz, T.; Rapp, B.E. Online monitoring of biofilm growth and activity using a combined multi-channel impedimetric and amperometric sensor. *Biosens. Bioelectron.* **2013**, *47*, 157–163. [[CrossRef](#)]
59. Stabryla, L.M.; Johnston, K.A.; Millstone, J.E.; Gilbertson, L.M. Emerging investigator series: It's not all about the ion: Support for particle-specific contributions to silver nanoparticle antimicrobial activity. *Environ. Sci. Nano* **2018**, *5*, 2047–2068. [[CrossRef](#)]
60. Arya, G.; Sharma, N.; Mankamna, R.; Nimesh, S. Antimicrobial silver nanoparticles: Future of nanomaterials. In *Microbial Nanobionics*; Springer: Berlin/Heidelberg, Germany, 2019; pp. 89–119. [[CrossRef](#)]
61. Mijndendonckx, K.; Leys, N.; Mahillon, J.; Silver, S.; Van Houdt, R. Antimicrobial silver: Uses, toxicity and potential for resistance. *Biometals* **2013**, *26*, 609–621. [[CrossRef](#)]
62. Dakal, T.C.; Kumar, A.; Majumdar, R.S.; Yadav, V. Mechanistic basis of antimicrobial actions of silver nanoparticles. *Front. Microbiol.* **2016**, *7*, 1831. [[CrossRef](#)]
63. Yamanaka, M.; Hara, K.; Kudo, J. Bactericidal actions of a silver ion solution on *Escherichia coli*, studied by energy-filtering transmission electron microscopy and proteomic analysis. *Appl. Environ. Microbiol.* **2005**, *71*, 7589–7593. [[CrossRef](#)] [[PubMed](#)]
64. Wirth, S.M.; Lowry, G.V.; Tilton, R.D. Natural organic matter alters biofilm tolerance to silver nanoparticles and dissolved silver. *Environ. Sci. Technol.* **2012**, *46*, 12687–12696. [[CrossRef](#)] [[PubMed](#)]
65. Goh, E.; Xu, X.; McCormick, P. Effect of particle size on the UV absorbance of zinc oxide nanoparticles. *Scr. Mater.* **2014**, *78*, 49–52. [[CrossRef](#)]
66. Radzig, M.; Nadtochenko, V.; Koksharova, O.; Kiwi, J.; Lipasova, V.; Khmel, I. Antibacterial effects of silver nanoparticles on gram-negative bacteria: Influence on the growth and biofilms formation, mechanisms of action. *Colloids Surf.* **2013**, *102*, 300–306. [[CrossRef](#)] [[PubMed](#)]
67. Sastry, M.; Mayya, K.S.; Bandyopadhyay, K. pH Dependent changes in the optical properties of carboxylic acid derivatized silver colloidal particles. *Colloids Surf. A Physicochem. Eng. Asp.* **1997**, *127*, 221–228. [[CrossRef](#)]
68. Ashraf, J.M.; Ansari, M.A.; Khan, H.M.; Alzohairy, M.A.; Choi, I. Green synthesis of silver nanoparticles and characterization of their inhibitory effects on AGEs formation using biophysical techniques. *Sci. Rep.* **2016**, *6*, 20414. [[CrossRef](#)]
69. Li, Y.; Xiao, P.; Wang, Y.; Hao, Y. Mechanisms and control measures of mature biofilm resistance to antimicrobial agents in the clinical context. *ACS Omega* **2020**, *5*, 22684–22690. [[CrossRef](#)]
70. Park, S.-H.; Kim, H.-S. Flash light-assisted facile and eco-friendly synthesis of platinum-based alloy nanoparticle/carbon nano-tube catalysts for a direct methanol fuel cell. *J. Electrochem. Soc.* **2014**, *162*, F204. [[CrossRef](#)]
71. Peulen, T.O.; Wilkinson, K.J. Diffusion of nanoparticles in a biofilm. *Environ. Sci. Technol.* **2011**, *45*, 3367–3373. [[CrossRef](#)]
72. Hadjipetrou, L.P.; Gray-Young, T.; Lilly, M.D. Effect of ferricyanide on energy production by *Escherichia coli*. *Microbiology* **1966**, *45*, 479–488. [[CrossRef](#)]

Disclaimer/Publisher's Note: The statements, opinions and data contained in all publications are solely those of the individual author(s) and contributor(s) and not of MDPI and/or the editor(s). MDPI and/or the editor(s) disclaim responsibility for any injury to people or property resulting from any ideas, methods, instructions or products referred to in the content.